

2013

Bed Sherwood Number and Chemical Kinetic Coefficient in a Fuel Reactor of Chemical Looping Combustion by Eulerian CFD Modeling

Ari Vepsäläinen

Lappeenranta University of Technology, LUT Energy, Finland

Srujal Shah

Lappeenranta University of Technology, LUT Energy, Finland

Petteri Peltola

Lappeenranta University of Technology, LUT Energy, Finland

Timo Hyppänen

Lappeenranta University of Technology, LUT Energy, Finland

Follow this and additional works at: http://dc.engconfintl.org/fluidization_xiv

 Part of the [Chemical Engineering Commons](#)

Recommended Citation

Ari Vepsäläinen, Srujal Shah, Petteri Peltola, and Timo Hyppänen, "Bed Sherwood Number and Chemical Kinetic Coefficient in a Fuel Reactor of Chemical Looping Combustion by Eulerian CFD Modeling" in "The 14th International Conference on Fluidization – From Fundamentals to Products", J.A.M. Kuipers, Eindhoven University of Technology R.F. Mudde, Delft University of Technology J.R. van Ommen, Delft University of Technology N.G. Deen, Eindhoven University of Technology Eds, ECI Symposium Series, (2013). http://dc.engconfintl.org/fluidization_xiv/101

This Article is brought to you for free and open access by the Refereed Proceedings at ECI Digital Archives. It has been accepted for inclusion in The 14th International Conference on Fluidization – From Fundamentals to Products by an authorized administrator of ECI Digital Archives. For more information, please contact franco@bepress.com.

BED SHERWOOD NUMBER AND CHEMICAL KINETIC COEFFICIENT IN A FUEL REACTOR OF CHEMICAL LOOPING COMBUSTION BY EULERIAN CFD MODELING

Ari Vepsäläinen^{a*}, Srujal Shah^a, Petteri Peltola^a and Timo Hyppänen^a
^aLappeenranta University of Technology, LUT Energy;
P.O.Box 20, FI-53850, Lappeenranta, Finland
*T: +358405654584; F: +358056216399; E: ari.vepsalainen@lut.fi

ABSTRACT

The transient Eulerian two-phase CFD model applying the kinetic theory of granular flow is used to simulate two pilot scale test balances in a fuel reactor of chemical looping combustion with methane as fuel and nickel-based oxygen carrier. The kinetic reaction rate coefficient of Nickel-based oxygen carrier particles is defined based on the measured total methane conversion, and correspondence with the experimental data was found. The bed Sherwood numbers were derived based on the CFD simulations. The derived Sh_{bed} correspond to the in-literature presented data, and explain the commonly faced problem of obtaining different chemical kinetic coefficients from the TGA and bench-scale fluidized bed reactor tests.

INTRODUCTION

A comprehensive review of the process research of chemical looping combustion (CLC) and oxygen carrier material development is provided by Adanez et al. (1). Feasible operation of chemical looping combustion with gaseous fuels has been proven in a pilot plant scale. Pröll et al. (2) reported stable operation of 120 kW_{th} CLC pilot plant with high conversion rates for gaseous fuel (methane) and nickel-based oxygen carrier (Fig. 1). In a technology development, the next demonstration scale is 1-3 MW_{th} (Adanez et al. (1)).

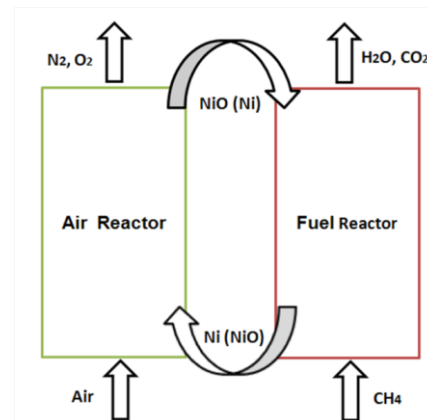


Figure 1 CLC process with methane combustion and NiO oxygen carrier

From a fundamental phenomenon perspective, the CLC process and the fluidized bed combustion processes differ in basic hydrodynamics due to the higher density of solid particles. Two-phase fluid dynamics controls heterogeneous mass transfer rates that have an influence on the chemical kinetic reaction rates. Also, the chemical kinetic coefficients of oxygen carriers differ from the conventional combustion processes. From the process efficiency perspective, both the air and the fuel reactors in CLC process should reach high total conversion rates within a wide load range. Thus, from a design point of view, both the chemical kinetics and the heterogeneous mass transfer knowledge are required for the scale-up of unit sizes.

In this work, the research focus is set on understanding the formation of effective reaction rate in a fuel reactor at the chemical looping combustion process. Commonly faced problem is that different heterogeneous mass transfer characteristics are reason for different chemical kinetic coefficients obtained from the TGA and bench-scale fluidized bed reactor tests, as discussed in Mattisson et al. (3) considering oxygen carriers used in chemical looping combustion process. Further, the scale-up of gas-solid contact related chemical conversion rates in the fluidized bed processes is far from simple and straightforward. This is discussed in Vepsäläinen et al. (4) regarding pilot and industrial scale coal combustion, and more generally in Leckner et al. (5) and Horio et al. (6).

The research approach here is Eulerian CFD modeling of methane combustion in a fuel reactor of CLC process. A number of validation studies focusing on the solid flow dynamics predicted by the Eulerian CFD models have been presented in literature. Benyahia et al. (7) showed comparison of the measured and the modeled time-averaged axial and horizontal solid volume fractions in a pilot scale fluid catalytic cracking (FCC) riser. A similar validation work focusing on circulating fluidized bed combustors has been presented by Shah et al. (8) for a cold pilot scale riser. Recently, the Eulerian CFD models have been also successfully applied for prediction of the heterogeneous mass transfer and reaction rates in fluidized beds. Cloette (9) presented multiphase Eulerian CFD simulation of fuel reactor in chemical looping combustion process operated under the bubbling bed regime with comparison to the measured (Pröll et al. (2)) axial gas conversion profiles. Chalermisinsuwan et al. (10) derived the axial Sherwood number profiles in a FCC reactor operating at fast fluidization regime by the Eulerian CFD modeling, and also highlighted the relationship of chemical kinetics and average mass transfer rate coefficient. Vepsäläinen et al. (11) derived bed Sherwood numbers for the bubbling and the circulating bed combustion conditions in a bench and a pilot scale reactor.

CFD MODELLING

Eulerian two-phase CFD Model

Two-phase Eulerian CFD simulations (Ansys Fluent 14) are based on the kinetic theory of granular flow. Table 1 shows the main sub-models and mesh design applied in the simulations. The continuity and momentum equations for one solid (NiO+Ni) and one gas phase are

$$\frac{\partial}{\partial t}(\alpha_g \rho_g) + \nabla \cdot (\alpha_g \rho_g \vec{u}_g) = \alpha_g S_g \quad (1.)$$

$$\frac{\partial}{\partial t}(\alpha_s \rho_s) + \nabla \cdot (\alpha_s \rho_s \vec{u}_s) = \alpha_s S_s . \quad (2.)$$

$$\frac{\partial}{\partial t}(\alpha_g \rho_g \vec{u}_g) + \nabla \cdot (\alpha_g \rho_g \vec{u}_g \vec{u}_g) = -\alpha_g \nabla p + \nabla \tau_g + \alpha_g \rho_g \vec{g} + K_{gs}(\vec{u}_s - \vec{u}_g) \quad (3.)$$

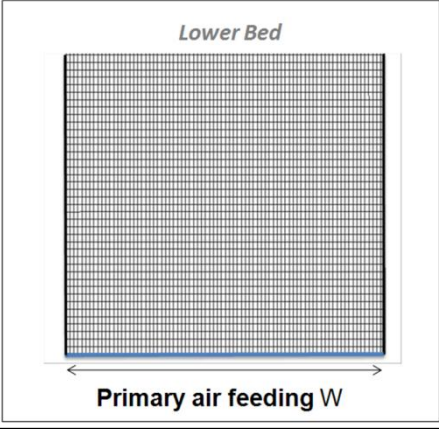
$$\frac{\partial}{\partial t}(\alpha_s \rho_s \vec{u}_s) + \nabla \cdot (\alpha_s \rho_s \vec{u}_s \vec{u}_s) = -\alpha_s \nabla p + \nabla \tau_s - \nabla p_s + \alpha_s \rho_s \vec{g} + K_{sg}(\vec{u}_g - \vec{u}_s). \quad (4.)$$

The species (i) conservation equation within phase (q) is given by

$$\frac{\partial}{\partial t}(\alpha_q \rho_q y_q^i) + \nabla \cdot (\alpha_q \rho_q \vec{u}_q y_q^i) = -\nabla \alpha_q J_q^i + r_q. \quad (5.)$$

Table 1 (a) Sub-models based on kinetic theory of granular flow (b) Mesh design

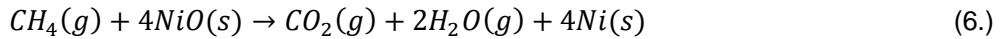
Gas-solid sub-models		Reactor Reactor depth (2D) = 1m, unit Cells No. cells in width W (0.159m) = 80 No. cells in height H (3m) = 800
Interphase momentum exchange coefficients	<i>Gidaspow et al.</i>	
Granular viscosity	<i>Syamlal et al.</i>	
Granular bulk viscosity	<i>Lun et al.</i>	
Frictional viscosity	<i>Schaeffer</i>	
Solids pressure	<i>Lun et al.</i>	
Radial distribution	<i>Lun et al.</i>	
Local granular temperature	<i>Algebraic</i>	
Turbulence model	<i>Standard k-epsilon dispersed multiphase</i>	
Solution methods time discretization space discretization	1 st order implicit 1 st order upwind	



Two test balances from the fuel reactor of 120 kW_{th} CLC prototype operation that are reported in Pröll et al. (2) are selected as a reference for the simulations. A two-dimensional reactor with width of 0.159 m and height of 3 m was constructed for the CFD simulations. The grid has 80 calculation cells in width and 800 cells in height. The mesh size is 1.99 x 3.75 mm², which corresponds to 14 and 28 times the particle diameter. The mesh size is fine enough as shown in CFD simulations of the same balances by Cloete et al. (9). Also, the mesh size selection criteria of 10 to 20 particle diameters have been reported in the literature (Andrews et al. (12); Benyahia (13)). The time step size of 0.001 s was applied. Temperature at the reactor was constant of 1174 K in both selected balances and constant properties of gases are applied for all gas species. Average gas density ρ_g of 3.6 kg/m³ and viscosity μ_g of 0.12·10⁻³ m²/s were applied. Diffusivity of methane D_{CH_4} is 0.12·10⁻³ m/s. Mean particle diameter of 0.135 mm is used.

Reaction sub-model

Combustion of methane is modeled by one overall heterogeneous reaction



Combustion reaction rate in species conservation equation (Eq. 5) is calculated from

$$R_{CH_4} = \frac{a_{NiO} C_{CH_4}}{\frac{1}{h_m} + \frac{1}{k_s}}, \quad (7.)$$

where k_s is apparent reaction rate constant of Nickel-based oxygen carrier. The surface area of oxygen carrier particles is given by

$$a_{NiO} = \frac{6\alpha_s}{d_p}. \quad (8.)$$

The local external convection mass transfer coefficient h_m is evaluated with a correlation of La Nauze and Jung (14) given by

$$Sh = \frac{h_m d_p}{D_{CH_4}} = 2 \alpha_g + 0.69(Re/\alpha_g)^{0.5} Sc^{0.33}. \quad (9.)$$

Simulation procedure

For all the simulated balances, first 5 seconds period was simulated from initial condition of constant solid volume fraction in a reactor to achieve stabilization of hydrodynamics, reaction rate and axial gas volume fractions. The stabilization period was then followed by 10 s analysis period simulation. The averaging of data for each balance was executed during the 10 s analysis period.

BED SHERWOOD NUMBER

Axial gas-to-particle mass transfer coefficient $\langle h_m \rangle$ profile was solved based on the axial, time-averaged and cross-section averaged, profiles of the CFD simulations as follows

$$\langle R_{CH_4} \rangle_{10s} = \frac{\langle a_{NiO} \rangle_{10s} \langle C_{CH_4} \rangle_{10s}}{\frac{1}{\langle h_m \rangle} + \frac{1}{k_s}}. \quad (10.)$$

Finally, bed Sherwood number is calculated from the average gas-to-particle mass transfer coefficient $\overline{h_m} = \int_0^h \langle h_m \rangle^{(\alpha_s)=0.15}$ in bed as follows

$$Sh_{bed} = \frac{\overline{h_m} d_p}{D_{CH_4}}. \quad (11.)$$

RESULTS AND DISCUSSION

A low (60 kW) and high load (120 kW) balances of fuel reactor reported in Pröll et al. (2) were selected to be simulated. Table 2 shows the basic operation conditions applied in these balances. The high load balance was modeled with the approximated fluidization velocity of 0.3 m/s. In a low load balance, the fluidization velocity is 0.17 m/s. Fig. 2 shows the simulated axial solid volume fraction profiles $\langle \alpha_s \rangle$ for the both of the balances. It also shows the measured solid volume fractions at two heights converted from the measured pressure profiles. Fig. 3 presents examples of instantaneous solid volume fractions from the two fluidization states. The low load balance is at the bubbling bed regime and the high load balance seems to be at the turbulent regime.

Table 2 Basic operational parameters for two simulated loads

Load	120 kW	60 kW
fluidization velocity u_f	0.3 m/s	0.17 m/s
solids loading m_{NiO}	22 kg	19 kg
average solid volume fraction in reactor α_s	0.11	0.093

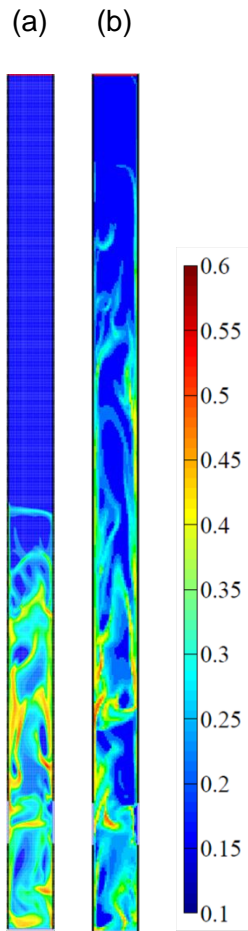


Figure 3 Instantaneous solid volume fractions: (a) low load and (b) high load balances.

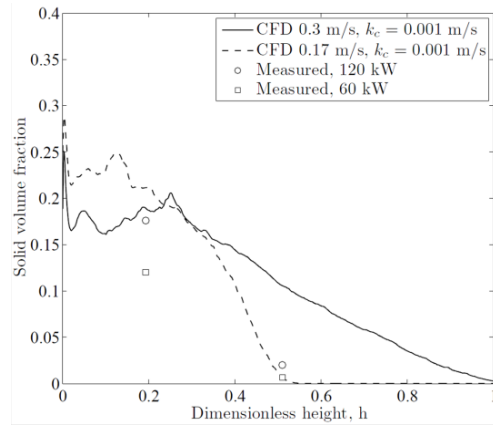


Figure 2 Axial solid volume fraction profiles

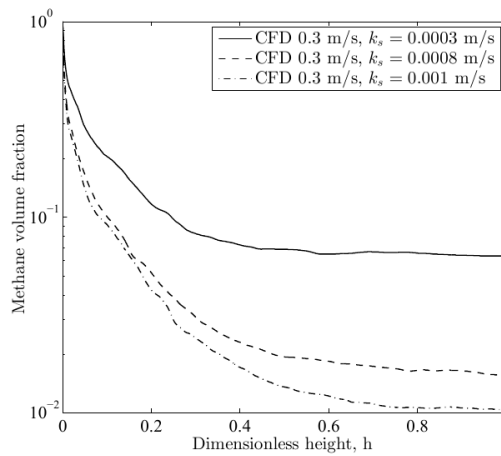


Figure 4 Effect of chemical kinetic coefficient on axial methane (CH_4) conversion profiles: high load balance.

First, the 0.3 m/s fluidization velocity balance was simulated with three different chemical kinetic reaction rate coefficients: Fig. 4 presents the resulted axial methane volume fraction $\langle y_{\text{CH}_4} \rangle$. For these balances, total methane conversions $X_{\text{CH}_4} = 1 - \dot{n}_{\text{CH}_4, \text{out}} / \dot{n}_{\text{CH}_4, \text{in}}$ are shown in Fig. 5. The chemical kinetic coefficients k_s of 0.001 m/s results the same total methane conversion X_{CH_4} of 0.97 as obtained from measurements (120 kW, Pröll et al. (2)). Secondly, the low load balance (60 kW) with 0.17 m/s fluidization velocity was then simulated with this chemical kinetic coefficient ($k_s = 0.001$ m/s). Fig. 5 shows that the resulted total methane conversion is higher than the measured one. It is also higher than the corresponding in high load balance, which is mainly due to lower flow rate of fluidization gas (Table 2). The same behavior was shown by CFD modeling reported in Cloete et al. (9).

A low load balance was simulated also with a lower chemical kinetic coefficient $k_s = 0.0006$ m/s, which resulted almost the same conversion rates as in the experiments. The lower total methane conversion measured at the low load balance could be explained by different of chemical reaction rate coefficients between the balances due to the different oxidation degree of NiO particles. Pröll et al. (2) reported that the oxidation degree X_{O_2} of NiO particles was 0.75-0.85 for low load balance and 0.5-0.6 for high load balance. Mattisson et al. (3) showed that reaction

rate constant of a nickel-based oxygen carrier decreases with increase of oxidation degree X_{O_2} as shown in Fig 6. Figure shows that a slight drop of chemical kinetic coefficient with oxidation degree is back-calculated by the Eulerian CFD simulations presented in this work. The behavior of the effective chemical kinetic coefficient k_s originates from the variation of grain sizes in NiO particle with oxidation degree.

Reactivity test (TGA or bench scale FB) data for the NiO oxygen carriers that were used in pilot scale experiments was not available. However, Mattisson et al. (3) presented kinetic data for NiO particles from a bench scale fluidized bed (ID 22 mm) experiments that varied with the oxidation degree in a range of 0.6-1.7 mol/(kgbars) at 850 °C. They also recalculated TGA reactivity test results of the same particles (Abad et al. (15)), and showed variance of kinetic coefficient from 0.11 to 0.2 mol/(kgbars). The chemical kinetic coefficient per surface area of spherical NiO particle k_s of 0.001 m/s corresponds to 0.33 mol/(kgbars) and k_s of 0.0006 m/s to 0.2 mol/(kgbars). As shown by Fig 6., the kinetic coefficients obtained by Eulerian CFD modeling of pilot scale reactor are very close to the ones obtained from TGA presented by Abad et al. (15).

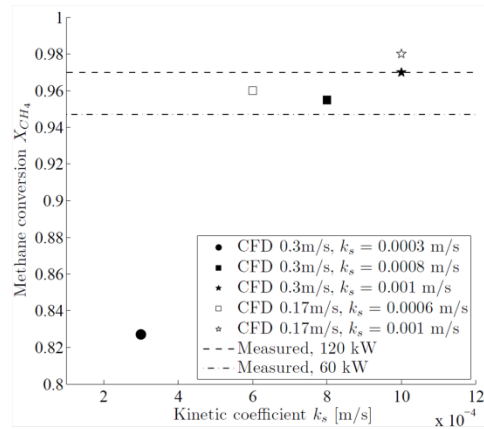


Figure 5 Simulated and measured total conversions of methane.

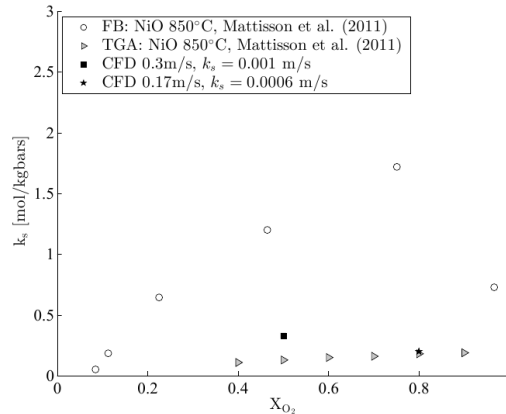


Figure 6 Chemical kinetic coefficient with oxidation degree of NiO

Average gas-to-bed mass transfer behavior in the fuel reactor was studied. Fig. 7 shows the bed Sherwood numbers Sh_{bed} (Eq. 11) against Reynolds number. An exponentially increasing trend of Sh_{bed} with Re can be seen for the CLC process as well as for FCC process with the similar chemical kinetic coefficients ($k_s = 0.0005$ - 0.0025 m/s) and particle size ($d_p = 0.075$ mm) obtained by Eulerian CFD modeling by Chalermisinsuwan and Piumsomboon (16). The exponential trend is similar to trend shown by experiments and CFD simulations with larger particles.

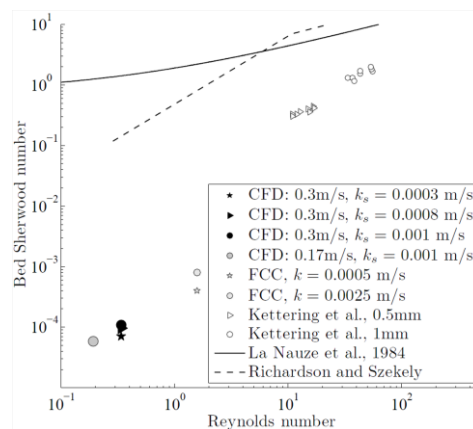


Figure 7 Bed Sherwood numbers against Reynolds numbers.

However, Fig. 7 highlights that the level of Sh_{bed} is several magnitudes of order lower than in e.g. combustion process (Vepsäläinen et al. (11)) for CLC and FCC processes, where particle size is small, chemical kinetic coefficient relatively high and all solids are active.

CONCLUSION

Chemical kinetic coefficients of NiO oxygen carriers that were derived by Eulerian CFD modeling correspond to the kinetic coefficients obtained from TGA tests (Abad et al. (15)). It was also found that the lower effective reaction rate of NiO particles observed in the test balances (Pröll et al. (2)) for low load balance could be explained by (1) decrease of the effective chemical kinetic with increase of oxidation degree of NiO particles (decrease of grain sizes) and (2) decrease of the gas-to-solid mass transfer rate (Sh_{bed}). The obtained kinetic coefficients k_s can be used in scale-up and process analysis related steady-state 1D and 3D CLC process models for the same oxygen carrier and oxidation degrees.

The derived bed Sherwood numbers are on the same level than reported in case of FCC process with the similar particle size and kinetic coefficients (Chalermsoonsuwan and Piumsomboon (16)). The bed Sherwood numbers also have the same response to increase of Reynolds number as shown by number of gas-to-solid mass transfer tests reported in literature (Fig. 7). For larger reactor sizes, bed Sherwood numbers Sh_{bed} can be obtained by a similar Eulerian CFD modeling approach as presented in this work, or an approximate value can be evaluated based on Reynolds number from Fig. 7.

ACKNOWLEDGMENT

The authors would like to acknowledge the financial support for this research from the Academy of Finland under grant 124368 and from the Carbon Capture and Storage Program (CCSP) coordinated by CLEEN Ltd. with funding from the Finnish Funding Agency for Technology and Innovation, Tekes.

NOTATION

a	surface area per volume, m^2/m^3	X_{CH_4}	methane conversion
C	concentration, mol/m^3	X_{O_2}	oxidation degree of NiO particle
D	diffusion coefficient, m^2/s	y	species volume fraction
d	diameter, m	W	width of reactor, m
g	gravity, m/s^2	$\langle x \rangle$	time and cross-section averaged
H	height of reactor, m	\bar{x}	$= \int_0^{h(\alpha_s)=0.15} \langle x \rangle$, average in bed
h_m	mass transfer coefficient, m/s	Greek letters	
J	Diffusion flux, kg/m^2s	α	volume fraction
K_{sg}	momentum exchange c., kg/m^3s	μ	viscosity, kg/sm
k_s	kinetic coefficient, $mol/kg_s; m/s$	ρ	density, kg/m^3
p	pressure, bar	τ	shear stress, N/m^2
Re	Reynolds number	Subscripts	
r	specific reaction rate, mol/m^2s	g,s	gas, solid phase
Sh	Sherwood number	p	particle
Sc	Schmidt number	t	time
u_f	fluidization velocity, m/s		

REFERENCES

1. J. Adanez, A. Abad, F. Garcia-Labiano, P. Gayan, L. F. de Diego. Progress in Chemical-Looping Combustion and Reforming technologies. *Prog. Energ. Combust. Sci.*, 38: 215-282, 2012
2. T. Pröll, P. Kolbitsch, J. Bolhàr-Nordenkampf, H. Hofbauer. A novel dual circulating fluidized bed system for chemical looping processes. *AIChE Journal*, 55(12): 3255-3266, 2009.
3. T. Mattisson, E. Jerndal, C. Linderholm, A. Lyngfelt. Reactivity of a spray-dried NiO/NiAl₂O₄ oxygen carrier for chemical-looping combustion. *Chem. Eng. Sci.*, 66: 4636-4644, 2011.
4. A. Vepsäläinen, K. Myöhänen, T. Hyppänen, T. Leino, A. Tourunen. Development and validation of a 3-dimensional cfb furnace model. In: *Proceedings of the 20th International Conference on Fluidized Bed Combustion*. 2009.
5. B. Leckner, P. Szentannai, F. Winter. Scale-up of fluidized-bed combustion - a review. *Fuel*, 90 (10): 2951–2964, 2011.
6. M. Horio, A. Nonaka, Y. Sawa, I. Muchi. A new similarity rule for fluidized bed scale-up. *AIChE Journal*, 32: 1466–1482, 1986.
7. S. Benyahia, H. Arastoopour, T.M. Knowlton, H. Massah. Simulation of particles and gas flow behavior in the riser section of a circulating fluidized bed using the kinetic theory approach for the particulate phase. *Pow. Tech.*, 112: 24-33, 2000.
8. S. Shah, J. Ritvanen, T. Hyppänen, S. Kallio. Space averaging on a gas-solid drag model for numerical simulations of a CFB riser. *Pow. Tech.* 218, 131–139, 2012.
9. S. Cloete, J. T. Stein, A. Shahriar. An assessment of the ability of computational fluid dynamic models to predict reactive gas–solid flows in a fluidized bed. *Pow. Tech.*, 215-216: 15-25, 2012.
10. B. Chalermsoonsuwan, P. Piumsomboon, D. Gidaspow. Kinetic theory based computation of PSRI riser: Part II —Computation of mass transfer coefficient with chemical reaction. *Chem. Eng. Sci.*, 64: 1212-1222, 2009.
11. A. Vepsäläinen, S. Shah, J. Ritvanen, T. Hyppänen. Bed Sherwood number in Fluidized Bed Combustion by Eulerian CFD Modeling. *Chem. Eng. Sci.*, 93: 206-213, 2013.
12. A. Andrews, P. Loezos, S. Sundaresan. Coarse-Grid Simulation of Gas-Particle Flows in Vertical Risers. *Ind. Eng. Chem. Res.*, 44: 6022-6037, 2005.
13. S. Benyahia. Fine-grid simulations of gas-solids flow in a circulating fluidized bed. *AIChE*, 58: 3589-3592, 2012.
14. R.D. La Nauze, K. Jung, J. Kastl. Mass transfer to large particles in fluidised beds of smaller particles. *Chem. Eng. Sci.*, 39 (11): 1623-1633, 1984.
15. A. Abad, J. Adánez, F. García-Labiano, L. F. Diego, P. Gayán, J. Celaya. Mapping of the range of operational conditions for Cu-, Fe-, and Ni-based oxygen carriers in chemical-looping combustion. *Chem. Eng. Sci.*, 62: 533-549, 2007.
16. B. Chalermsoonsuwan, P. Piumsomboon. Computation of the mass transfer coefficient of FCC particles in a thin bubbling fluidized bed using two- and three-dimensional CFD simulations. *Chem. Eng. Sci.*, 66: 5602-5613, 2011.